Electronic transport in a quantum wire under external terahertz electromagnetic irradiation

Guanghui Zhou,[1,2,3,*] Mou Yang,[2] Xianbo Xiao,[2] and Yuan Li[2]
[1]*CCAST (World Laboratory), PO Box 8730, Beijing 100080, China*
[2]*Department of Physics, Hunan Normal University, Changsha 410081, China*
[3]*International Center for Materials Physics, Chinese Academy of Sciences, Shenyang 110015, China*
(Received 1 May 2003; revised manuscript received 5 June 2003; published 15 October 2003)

We theoretically study the electronic transport of a straight quantum wire partly irradiated under an external terahertz electromagnetic field at low temperature. Using the free-electron model and the scattering matrix approach, we demonstrate that although the electrons in a ballistic quantum wire only suffer from lateral collisions with photons, the reflection of electrons also takes place. Interestingly, when the frequency of the electromagnetic field is resonant with the separation of lateral energy levels of the wire, there is a sharp step structure in the electronic transmission probability as a function of the total energy of the electron or the strength of the field. The physical origin of this phenomena is the electron intersubband transition when a finite-range transversely polarized electromagnetic field irradiates a quantum wire. The interference pattern also appears in the electronic transmission probability as a function of the field-irradiated length.

DOI: 10.1103/PhysRevB.68.155309 PACS number(s): 73.23.−b, 73.21.Hb, 78.67.Lt

I. INTRODUCTION

In recent years mesoscopic physics has been extensively studied due to its potential application in the future. Nowadays the increasingly progressive arts and crafts of nanotechnologies allow researchers to realize some real mesoscopic systems in laboratory. One can confine two-dimensional electron gas in an ultranarrow channel on a $GaAs/Al_xGa_{1-x}As$ heterojunction[1] by applying a confinement potential and obtain an ideal one-dimensional (1D) interacting electron system or a 2D quantum point contact (short quantum wire). Recently, a 3D metallic nanowire has been constructed when the probe pin is apart from a metal film.[2] Depending on the nature of the materials, a quantum wire can be as long as up to 100 nm (long quantum wire) and this size may still be comparable to the Fermi wavelength of electrons. In the ballistic regime and at low temperatures the quantum coherent effect will dominate the electronic transport properties of these low-dimensional systems. The basic feature is that the conductance shows a histogram structure when the lateral size of the wire varies and each step has a height of $2e^2/h$ or an integer times it.[3] The interaction of electrons in 1D quantum wires induces transport anomalies. The perfect realization of a 1D system provides a new type of quantum liquid (Tomonaga-Luttinger liquid), which shows strongly correlated features as demonstrated by the techniques such as bosonization.[4] Furthermore, the electronic transport properties of quantum wires can be affected by many other factors. The presence of disorders in quantum wires leads to a suppression of the conductance plateaus below integer values,[3,5] and the coupling among wire and reservoirs (leads) has also been accounted for.[6] Geometrically, the varying of the wire lateral shape yields a mixture of different modes. If the shape varies slowly enough to satisfy the adiabatic approximation, the staircase structure of conductance is still preserved, but it is totally determined by the narrowest neck part of the whole wire.[7]

Recently, an interesting topic about time-dependent quantum transport has been widely carried on for quantum wire systems, such as the presence of a finite-range time-modulated potential,[8] quantum pumping,[9] etc. Furthermore, when a quantum wire is irradiated under a coherent external electromagnetic (EM) field,[10–18] many new features arise because of the inelastic scattering by photons. The typical values of the lateral energy level separation and the Fermi energy are of the order of 1–100 meV for quantum wires. This corresponds to matching frequencies of the order of 1–100 THz, which are available in experiments with the development of ultrafast laser technology.[19] When the Fermi level is below the lowest lateral level in the neck part of wire, electrons cannot go though without the assistance of external fields. However, under external field irradiation, electrons can absorb the energy of photons and go though this geometric barrier.[10–13] Therefore, in the regime of the barrier the electron reflection may be induced by the combination effect of external field and lateral shape variation.[10–16] However, the pure external EM field effect (extracting the wire neck effect) on the electron transport of a straight quantum wire has drawn less attention. And this effect may be important for the understanding of basic physics and for nanoscale circuit applications in the future. Recently, Ref. 17 studied quantum transport in a straight quantum wire irradiated by a longitudinal EM field within a finite range. Up to now, to our knowledge, the influence of transversely polarized EM field on a straight quantum wire has only been studied with a δ-profile range of the field.[18]

In this paper, we study the quantum transport property of a straight long quantum wire (either a 2D semiconductor quantum wire or a 3D metallic one) irradiated under a finite-range transversely polarized THz EM field. The transversely polarized field results in intersubband transitions, whereas the longitudinally polarized field results in intrasubband transitions. When an external field transversely irradiates the finite range of a straight quantum wire, the displacement symmetry along the wire is violated so that longitudinal momentum is not a conservative quantity and reflection must arise in general. Moreover, when the range of the field is assumed to be comparable with the phase-breaking length of

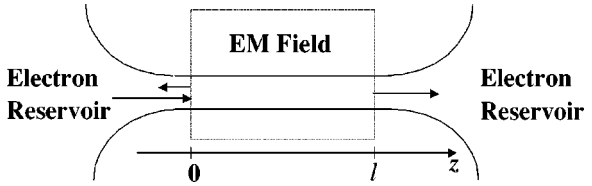

FIG. 1. Sketch configuration of the system as an external electromagnetic field irradiates the middle part of a straight quantum wire connecting two reservoirs. The arrows denote the propagation directions of electrons.

electrons the entire transmission process is coherent and can be described by a time-dependent Schrödinger equation, the two reservoirs at both ends of the quantum wire can be taken to be free from time-modulation effects so that the distribution of incident electrons is well determined. Thus the quantum transport in the presence of a finite-range field can be cast into a Landauer-Büttiker-type formalism.[17] So we will use the method of time-dependent mode matching and scattering matrix in this work. We demonstrate that the finite-range EM field effect on a straight quantum wire is similar to that of a barrier which yields an electron reflection from lateral collisions of electrons with photons. A new feature is that a sharp step structure of the resonant transmission probability appears as the total electron energy or the strength of the field increases to a threshold value due to the effect of electronic wave vector split induced by the coherent EM field. This new phenomenon has not been predicted previously for such a straight quantum wire system.

In Sec. II we present the formulation for solving the time-dependent Schrödinger equation of the system. In Sec. III we study the electronic transmission properties of the system by means of the scattering matrix and present some numerical examples. And finally, Sec. IV presents a summary and conclusion.

II. MODEL AND FORMALISM

The system under investigation is sketched in Fig. 1, where a 3D model system consists of a straight quantum wire connecting two reservoirs. The longitudinal z axis is along the wire, and the x and y axes are in the transverse directions. A THz EM field with the wave vector along the x axis transversely irradiates a finite range ($0 \leqslant z \leqslant l$) of the wire in an unspecified way. The field is described by the vector potential

$$\vec{A}(t) = \frac{\varepsilon}{\omega} \cos \omega t \cdot \hat{e}_y, \tag{1}$$

where ω and ε are the angular frequency and amplitude of the field, respectively, and $\hat{e}_y$ is the unit vector in the y direction (polarized direction). At low temperature and in the ballistic regime we adopt the free-electron model. Therefore, the time-dependent Schrödinger equation in the field-irradiated part of the wire is

$$[(\hat{p} + e\vec{A})^2 + U(x,y)]\Psi(x,y,z,t) = i\frac{\partial}{\partial t}\Psi(x,y,z,t), \tag{2}$$

where the atomic unit is adopted (i.e., $\hbar = 2m^* = 1$), $\hat{p} = -i\nabla$ is the momentum, and the potential $U(x,y)$ is in the form of either a hard-wall potential or a parabolic one which confines electrons to the wire and to the reservoirs.

We assume that the electronic wave function in Eq. (2) has a separation form

$$\Psi(x,y,z,t) = \sum_k e^{ikz} \sum_n a_n(t)\phi_n(x,y), \tag{3}$$

where k is the longitudinal momentum and $a_n(t)$ presents the time-dependent state amplitudes. $\phi_n(x,y)$ are the eigenfunctions of the transverse motion without an EM field, which is dependent on the specified confining potential $U(x,y)$. For simplicity we only consider the transition between the two lowest transverse (lateral) energy levels with the Fermi level between them and ignore other higher levels (i.e., use the two-level approximation). Substituting ansatz (3) into Eq. (2) and neglecting the $\sim A^2$ term (this term only gives an extra phase that is common to all modes) we obtain an equation of the matrix form

$$i\frac{\partial}{\partial t}\begin{bmatrix} a_1 \\ a_2 \end{bmatrix} = \begin{bmatrix} \epsilon_1 + k^2 & iM\cos\omega t \\ -iM\cos\omega t & \epsilon_2 + k^2 \end{bmatrix}\begin{bmatrix} a_1 \\ a_2 \end{bmatrix}, \tag{4}$$

where ϵ_1 and ϵ_2 are the eigenvalues of the two transverse modes and M is a coupling parameter of the two modes and the EM field (interaction energy),

$$M = \frac{2e\varepsilon}{\omega}\left|\int \phi_1^* \frac{\partial}{\partial y}\phi_2 dxdy\right| = \frac{2e\varepsilon}{\omega}\left|\int \phi_2^* \frac{\partial}{\partial y}\phi_1 dxdy\right| \sim \varepsilon/\omega, \tag{5}$$

which is proportional to the field strength and inversely proportional to frequency. Except for an additional k^2 in the diagonal elements of the interaction matrix, Eq. (4) is the same as the equation of a two-level atom interaction with a single-mode light field. Inspired by the treatment of the two-level atom interaction with a coherent light field,[20] we use a time-dependent unitary transformation and the rotating-wave approximation to reduce Eq. (4) to being time independent. Thus using the associated inverse transformation we finally obtain the time-dependent electronic wave function

$$\Psi(x,y,z,t) = \sum_k [C_{k,+}|+\rangle e^{-i(\lambda_+ + k^2)t} + C_{k,-}|-\rangle e^{-i(\lambda_- + k^2)t}]e^{ikz}, \tag{6}$$

where $\lambda_\pm = \pm\frac{1}{2}\sqrt{\delta^2 + M^2}$ is the eigenvalues of the time-independent interaction matrix after the unitary transformation, $\delta = \omega - (\epsilon_2 - \epsilon_1)$ is the detuning of the field frequency with the two lateral energy separation, and $|\pm\rangle$ are the two vectors defined as

$$|\pm\rangle = \begin{bmatrix} e^{-i(\epsilon_1 + k^2 - \delta/2)t} \\ A_\pm e^{-i(\epsilon_2 + k^2 + \delta/2)t} \end{bmatrix}, \quad A_\pm = \frac{1}{M}(-\delta \pm \sqrt{\delta^2 + M^2}). \tag{7}$$

By using the above electronic wave function expressed by Eqs. (6) and (7), we can analyze the electronic transmission as a function of the electron total energy and EM field parameters such as the frequency and amplitude.

III. ELECTRONIC TRANSMISSION

First, we consider electronic transmission through the left interface (boundary) between regions with field and without field irradiation. The transmission property for the right interface can be obtained symmetrically.[21] The electron wave function in the unirradiated left part of the wire can be simply written as

$$\Psi(z<0)=\begin{bmatrix} e^{i(k_1 z-Et)}+C_1 e^{-i(k_1 z+Et)} \\ C_2 e^{-i[k_2 z+(E+\omega)t]} \end{bmatrix}, \tag{8}$$

where we have assumed that the electron emits from left to right with total energy E, unitary amplitude, and momentum $k_1=\sqrt{E-\epsilon_1}$. Here $k_2=\sqrt{E-\epsilon_2+\omega}$, and C_1 and C_2 are the reflection coefficients of the two modes. Therefore, according to Eq. (6), the electron wave function in the regime of $z>0$ can be written as

$$\begin{aligned}\Psi(z>0)&=C_+|+\rangle e^{ik_+ z}e^{-i(\lambda_+ +k_+^2)t} \\ &\quad +C_-|-\rangle e^{ik_- z}e^{-i(\lambda_- +k_-^2)t} \\ &=\begin{bmatrix} C_+ e^{i(k_+ z-Et)}+C_- e^{i(k_- z-Et)} \\ A_+ C_+ e^{i[k_+ z-(E+\omega)t]}+A_- C_- e^{i[k_- z-(E+\omega t)]} \end{bmatrix},\end{aligned} \tag{9}$$

where $C_\pm$ are the transmission coefficients of the two modes and

$$k_\pm=\sqrt{E-\epsilon_1+\frac{\delta}{2}-\lambda_\pm} \tag{10}$$

are the two field-spilt electron wave vectors (momenta), from which one can infer that the Rabi oscillation in space (along the z axis) arises in the field part of the wire between these two states with wavelength $2\pi/(k_- -k_+)$. Now we can match the wave functions at the boundary $z=0$ (i.e., let the two wave functions and their differentials be continuous) to determine the four constants C_+, C_-, C_1, and C_2 and to calculate the transmission probability of the single-left-interface case.

In the following numerical examples, for simplicity we select the first lateral energy ϵ_1 as the energy unit, $1/\epsilon_1$ as the time unit, and $1/(2\pi\sqrt{\epsilon_1})$ as the length unit. The calculated transmission probability versus detuning $\delta(\sim\omega)$ is shown in Fig. 2 with the two sets of parameters as described in the caption. The dashed curve for $M=0.15\epsilon_1$ remains almost constant even at resonant frequency as the situation without an external field. The reason is that in the case of small mode coupling M both spilt modes in the field-irradiated part are propagating and all contribute to the transmission (see the next paragraph). As M increases the resonant peak appears. In the regime of $|\delta|>0.3$, the transmission probability for

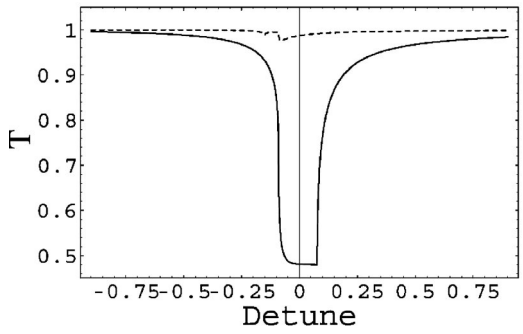

FIG. 2. Transmission probability vs detuning $\delta=\omega-(\epsilon_2-\epsilon_1)$ for one boundary with the parameters of $\epsilon_1=1$, $\epsilon_2=2\epsilon_1$, and $E=1.2\epsilon_1$, in the case of $M=0.4\epsilon_1$ (solid line) and $M=0.15\epsilon_1$ (dashed line), respectively.

$M=0.4\epsilon_1$ (solid curve) remains unchanged, but it decreases rapidly from near 1 to 0.5 as δ is approaches zero (resonant case $\omega\simeq\epsilon_2-\epsilon_1$). One can see that a resonant structure turns up but its shape is different from that of the EM field resonant absorption of an atom.[20] We note that if $\omega\to 0$, the field is reduced to the static magnetic field situation which has been discussed previously.[22]

Since the main physics may appear at the vicinity of the resonant frequency, we only give results for the resonant case ($\delta=0,\lambda_\pm=\pm M/2$) in the following arguments. In the resonant case the transmission matrix t' and the reflection matrix r for the left interface are simply expressed as

$$t'=\begin{bmatrix} k_1/(k_1+k_+) & 0 \\ k_1/(k_1+k_-) & 0 \end{bmatrix}, \tag{11}$$

$$r=\begin{bmatrix} (k_1^2-k_+k_-)/[(k_1+k_+)(k_1+k_-)] & 0 \\ k_1(k_- -k_+)/[(k_1+k_+)(k_1+k_-)] & 0 \end{bmatrix}, \tag{12}$$

respectively. Thus the transmission probability for the left interface can be derived analytically,

$$\begin{aligned}T&=2\sum_k \left|\frac{\sqrt{k_1 k}}{k_1+k}\right|^2\theta(k^2) \\ &=2\left|\frac{\sqrt{k_1 k_+}}{k_1+k_+}\right|^2\theta(k_+^2)+2\left|\frac{\sqrt{k_1 k_-}}{k_1+k_-}\right|^2\theta(k_-^2),\end{aligned} \tag{13}$$

where $\theta(x)$ is the step function and the two split wave vectors are simply reduced to $k_\pm=\sqrt{E-\epsilon_1\mp M/2}$ according to Eq. (10). The solid line in Fig. 3 shows the transmission probability versus the total energy E in the resonant case according to Eq. (13) with parameters of $\epsilon_1=1$, $\epsilon_2=2$, and $M=0.4\epsilon_1$. One can clearly see that the transmission is almost blocked by the EM field when the electron energy is near ϵ_1. Interestingly, there is a step arising for the transmission as the energy increases to $E=\epsilon_1+M/2$, and this pure external field effect cannot be obtained for straight quantum wires irradiated under a longitudinally polarized EM field[17] and for the neck shape wires[10–15] even in the case of transversely polarized EM field irradiation. In our case of a straight quantum wire, when electrons penetrate though the interface to the field-irradiated region, the transverse levels of the electrons in wires are dressed and one electron mode is

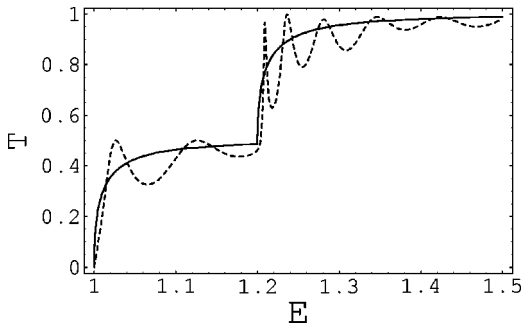

FIG. 3. Transmission probability in the resonant case vs total electron energy (in units of ϵ_1) with $\epsilon_1=1$, $\epsilon_2=2\epsilon_1$, and $M=0.4\epsilon_1$. The solid curve for the case of one boundary only and the dashed curve for the case of two boundaries with an irradiation length of $l=33$, respectively.

split into two time-dependent modes $|+\rangle e^{-i(M/2+k_+^2)t}$ and $|-\rangle e^{-i(-M/2+k_-^2)t}$ with longitudinal momenta k_+ and k_-, respectively. Further, when $E<\epsilon_1+M/2$ k_+ is imaginary, the mode $|+\rangle e^{-i(M/2+k_+^2)t}$ corresponds to an evanescent (nonpropagating) mode which contributes nothing to the transmission so that the total transmission probability is suppressed to near 0.5. When $E>\epsilon_1+M/2$ both modes become propagating and all contribute to the transmission. Therefore, the transmission step occurs at the point of $E=\epsilon_1+M/2$. Moreover, when $E\gg\epsilon_1+M/2$ the field is comparably too weak to affect the system, so in this case the transmission probability is close to 1 as that without an external field. This effect of splitting wave vectors originally comes from the intersubband transition. The solid curve in Fig. 4 shows the transmission probability versus interaction energy $M(\sim\varepsilon)$ in the resonant case with parameters of $\epsilon_1=1$, $\epsilon_2=2$, and $E=1.2\epsilon_1$. Similarly, there is a step dropping for the transmission probability. When M is small the transmission probability decreases gradually starting from 1, and it drops to 0.5 rapidly as M reduces to 0.4 and then it decreases linearly and slowly as M increases. This step structure of the transmission probability has the same physical origin as that mentioned above.

The transmission probability for the off-resonant general

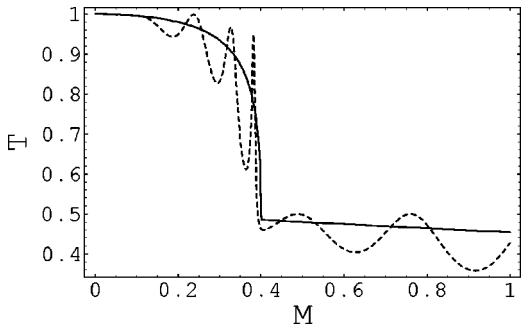

FIG. 4. Transmission probability in the resonant case vs interaction energy M with $\epsilon_1=1$, $\epsilon_2=2\epsilon_1$ and $E=1.2\epsilon_1$. The solid curve for the case of one boundary only and the dashed curve for the case of two boundaries with an irradiation length of $l=33$, respectively.

case can be carried out without difficulty in principle but we do not give the detailed result here.

Next, we consider the electronic transmission of the whole wire. In this case the system contains two interfaces between regions with and without field irradiation. To obtain the total transmission through the two interfaces with a length of field irradiation range l (see Fig. 1), we use the approach recently developed by Torres and Saénz.[22] This approach needs to derive the total scattering matrix which can be expressed in the transmission matrix and reflection matrix on each boundary. Because of the similarity of the two interfaces, one does not have to match the wave functions at the right boundary. The total transmission matrix is just the antidiagonal submatrix of the total scattering matrix in the symmetrical system case. Detailed knowledge about this aspects is referred to Ref. 22 and is not presented here. After some manipulation one can obtain the total transmission matrix

$$t_{total}=t(1-Ur'Ur')^{-1}Ut', \quad U=\begin{bmatrix} e^{ik_+l} & 0 \\ 0 & e^{ik_-l} \end{bmatrix}, \tag{14}$$

where t' (t) is the transmission matrix from left (right) to right (left) and r' is the reflection matrix from right to left for the first interface as implicated in Eqs. (11) and (12), and U is the propagation matrix between the two interfaces (field-irradiated region). Therefore the total transmission probability reads

$$T=\mathrm{Tr}[t_{total}^{\dagger}t_{total}]=P_1+P_2, \tag{15}$$

where P_1 and P_2 are the population of electrons occupying the lower and upper modes, respectively. The detailed calculation gives

$$P_1=\left|\frac{2k_1k_+}{e^{-ik_+l}(k_1+k_+)^2-e^{ik_+l}(k_1-k_+)^2}+\frac{2k_1k_-}{e^{-ik_-l}(k_1+k_-)^2-e^{ik_-l}(k_1-k_-)^2}\right|^2,$$

$$P_2=\left|\frac{2k_1k_+}{e^{-ik_+l}(k_1+k_+)^2-e^{ik_+l}(k_1-k_+)^2}-\frac{2k_1k_-}{e^{-ik_-l}(k_1+k_-)^2-e^{ik_-l}(k_1-k_-)^2}\right|^2. \tag{16}$$

The dashed curves in Figs. 3 and 4 show the calculated total transmission probability as a function of E and M with $l=33$ (other parameters are the same as those of corresponding dashed curves) according to Eqs. (15) and (16), respectively. One can see that for the same reason the two curves also have a step structure at point $E=\epsilon_1+M/2$ and $M=0.4\epsilon_1$, respectively. However, it apparently shows an interference pattern. As the length of the field irradiation range l is an integer time of π/k_-, peaks appear. One can find that the dashed curve is just the solid one superimposed with

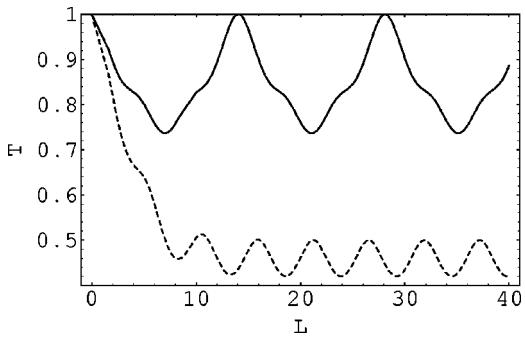

FIG. 5. Transmission probability in the resonant case vs field irradiating length l with $\epsilon_1=1$, $\epsilon_2=2\epsilon_1$, and $M=0.4\epsilon_1$. The solid curve for $E=1.25\epsilon_1$ and the dashed curve for $E=1.15\epsilon_1$, respectively.

some interference pattern due to the interference of the forward-going wave and backward-going wave in the field-irradiated part of the wire.

Finally, we consider the electronic transmission as a function of the field irradiation length l in the resonant case. Figure 5 shows the calculated transmission probability versus l with parameters of $\epsilon_1=1$, $\epsilon_2=2\epsilon_1$, and $M=0.4\epsilon_1$, the solid curve for $E=1.25\epsilon_1$ and the dashed curve for $E=1.15\epsilon_1$, respectively. The solid curve shows a nonstandard sine oscillation pattern. The reason is that in this set of parameters the two modes in the field-irradiated region are all propagating, which results in an interference effect for the electronic transmission. The first interference peak appears at $l=\pi/k_+\approx 14.1$. The dashed curve corresponds to the situation that only the k_- mode is propagating, so that the transmission probability decays from 1 to 0.5 in the range of $0<l<8$; then, it becomes a standard sine oscillation with period of $\pi/k_-\approx 5.6$. Therefore, the quantum tunneling happens in the range of $0<l<8$ and we can neglect its tunneling effect when $l\gg 8$ for this particular system.

From the above demonstration, we know that the electronic transmission through a finite-range transversely polarized EM-field-irradiated straight quantum wire has a sensitive response to both external field strength and frequency. This point makes the prospect of using quantum wire devices as photon detectors[10,19,23] at the THz frequency range quite possible. THz frequencies remain one of the most undeveloped frequency ranges in the electromagnetic spectrum. Present technology uses either superconductor-insulator-superconductor junctions or Schottky diodes for the THz detection.[19] Both devices are tunnel devices; thus they have large values of specific capacitance due to the sandwich geometry. This large junction capacitance is harmful to high-frequency applications. In quantum wire devices, however, this capacitive shunting will not be a serious problem.

IV. DISCUSSION AND SUMMARY

The analytical calculation in this paper is independent of the characteristics of the materials of the quantum wire. It is a general scheme for any straight quantum wire which suits the free-electron model. For a 2D semiconductor quantum wire formed[1] on high-mobility GaAs/$Al_{1-x}Ga_xAs$, the typical Fermi energy $E_F\simeq 9$ meV and the first lateral level $\epsilon_1=4$ meV (dependent on the gate voltage). Thus the second level is 16 meV if a 2D hard confining potential is adopted. The separation between them is 12 meV, so the relevant resonant external field frequency is about 12 THz. For a 3D metallic nanowire the transverse level separation is larger and the frequency of the resonant field will be higher (near-infrared regime). Moreover, in our calculation we even did not specify the type of confining potential. The different confining potential (either a hard-wall potential or a parabolic potential) results in different transverse eigenfunctions ϕ_n in Eq. (3), whereas it only affects the interaction energy parameter M and the behavior of the transmission will be the same qualitatively.

In summary, using the free-electron model and the method of time-dependent mode matching and scattering matrix, we have theoretically studied the electronic transmission property of a straight quantum wire irradiated under a finite-range transversely polarized THz EM field. We have demonstrated that the reflection will arise when the electrons only suffer from lateral collisions with photons. The electronic transmission probability as a function of field frequency shows an apparent asymmetric absorption peak. In the case in which the field frequency is resonant with lateral level separation, the transmission probability always displays an interesting step structure when either the total electron energy E or interaction energy M increases to a threshold value. The physical origin is the electronic intersubband transition when a transversely polarized electromagnetic field irradiates the finite range of a quantum wire. The transmission probability as a function of irradiation length also shows an interference structure. More detailed studies of these systems are worth continuing for a better understanding of THz wave interactions with matter.[19]

ACKNOWLEDGMENT

This work was supported by the Nature Science Foundation of Hunan (Grant No. 02JJY2008).

*Electronic address: ghzhou@hunnu.edu.cn

[1] B.J. van Wees, H. van Houten, C.W.J. Beenakker, J.G. Williamson, L.P. Kouwenhoven, D. van der Mare, and C.T. Foxon, Phys. Rev. Lett. **60**, 848 (1988).

[2] J.M. Krans, J.M. Ruitenbeek, V.V. Fisum, I.K. Yanson, and L.J. Jongh, Nature (London) **375**, 767 (1995).

[3] A. Szafer and A.D. Stone, Phys. Rev. Lett. **62**, 300 (1989); G. Rubio, N. Agrait, and S. Vieira, *ibid.* **76**, 2302 (1996).

[4] A. Luther and I. Peschel, Phys. Rev. B **9**, 2911 (1974); O.P. Sushkov, Phys. Rev. B **64**, 155319 (2001).

[5] X.R. Wang, Yupeng Wang, and Z.Z. Sun, Phys. Rev. B **65**, 193402 (2002).

[6] K.I. Imura, K.V. Pham, P. Lederer, and F. Piéchon, Phys. Rev. B **66**, 035313 (2002).
[7] C.A. Stafford, D. Baeriswyl, and J. Bürki, Phys. Rev. Lett. **79**, 2863 (1997).
[8] C.S. Tang and C.S. Chu, Phys. Rev. B **53**, 4838 (1996); Wenjun Li and L.E. Reichl, *ibid.* **60**, 15 732 (1999).
[9] P.W. Brouwer, Phys. Rev. B **58**, R10 135 (1998); E.R. Mucciolo, C. Chamon, and C.M. Marcus, Phys. Rev. Lett. **89**, 146802 (2002).
[10] Q. Hu, Appl. Phys. Lett. **62**, 837 (1993); S.C. Feng and Q. Hu, Phys. Rev. B **48**, 5354 (1993).
[11] L.Y. Gorelik, A. Grincwajg, V.Z. Kleiner, R.I. Shekhter, and M. Jonson, Phys. Rev. Lett. **73**, 2260 (1994).
[12] O. Tageman, L.Y. Gorelik, R.I. Shekter, and M. Jonson, J. Appl. Phys. **81**, 285 (1997).
[13] S. Blom, L.Y. Gorelik, M. Jonson, and R.I. Sheckhter, Phys. Rev. B **58**, 16 305 (1998).
[14] O. Tageman and A.P. Singh, Phys. Rev. B **60**, 15 937 (1999).
[15] S. Blom and L.Y. Gorelik, Phys. Rev. B **64**, 045320 (2001).
[16] M.R. Black, Y.M. Lin, S.B. Cronin, O. Rabin, and M.S. Dresselhaus, Phys. Rev. B **65**, 195417 (2002).
[17] C.S. Tang and C.S. Chu, Phys. Rev. B **60**, 1830 (1999).
[18] C.S. Chu and C.S. Tang, Solid State Commun. **71**, 119 (1996).
[19] B. Ferguson and X.C. Zhang, Nat. Mater. **1**, 26 (2002).
[20] *Quantum Optics*, edited by D. F. Walls and G. J. Milburm (Springer-Verlag, Berlin, 1994).
[21] E.N. Bogachek, A.G. Scerbakov, and U. Landman, Phys. Rev. B **53**, R13 246 (1996).
[22] J.A. Torres and J.J. Saénz, cond-mat/0012250 (unpublished).
[23] A.A. Ignatov and A.P. Jauho, J. Appl. Phys. **85**, 3643 (1999).